PROBLEMY MECHATRONIKI
UZBROJENIE, LOTNICTWO, INŻYNIERIA BEZPIECZEŃSTWA

ISSN 2081-5891

8, 4 (30), 2017, 47-60

PROBLEMS OF MECHATRONICS
ARMAMENT, AVIATION, SAFETY ENGINEERING

Sliding Mode Control for a Gyroscope System

Izabela KRZYSZTOFIK*, Zbigniew KORUBA

Kielce University of Technology,
7 Tysiąclecia Państwa Polskiego Avenue, 25-314 Kielce, Poland
** Corresponding author's email address: pssik@tu.kielce.pl*

Received by the editorial staff on 18 October 2016.
Reviewed and verified version received on 11 February 2017.

DOI 10.5604/01.3001.0010.7317

Abstract. This paper presents a mathematical model of a gyroscope system with a sliding mode controller. A comparative analysis based on various control algorithms implemented in a controlled gyroscope system installed on a mobile platform (such as an UAV or a homing rocket missile) proved that sliding mode control can be highly effective, especially when external input interferences exist with the kinematic reactions of the mobile platform. A gyroscope system with a sliding mode controller can be used in the optical target seeker systems of precision weapons. The simulation results are provided in a graphical format.
Keywords: mechanical engineering, controlled gyroscope, sliding mode controller, dynamics, control

This work has been compiled from a paper presented during the 11th International Armament Conference on *Scientific Aspects of Armament and Safety Technology*, Ryn, Poland, 19-22 September 2016.

1. INTRODUCTION

Observation, targeting and tracking systems share one core component, known as the target seeker, or simply the seeker, the primary function of which is to determine the target line of sight (T-LOS). Most seeker systems are installed on mobile platforms, such as aboard homing missiles, UAVs, and mobile missile launchers. In these environments, the seekers are exposed to deterministic interactions and random interactions [1, 2]. This paper describes a T-LOS control and stabilizing system, operated under deterministic and random interactions, in the form of a gyroscope system (GS). The operating precision of the GS determines the accuracy of the seeker.

Figure 1 gives a simplified functional scheme of a gyroscope seeker system installed on a homing air platform.

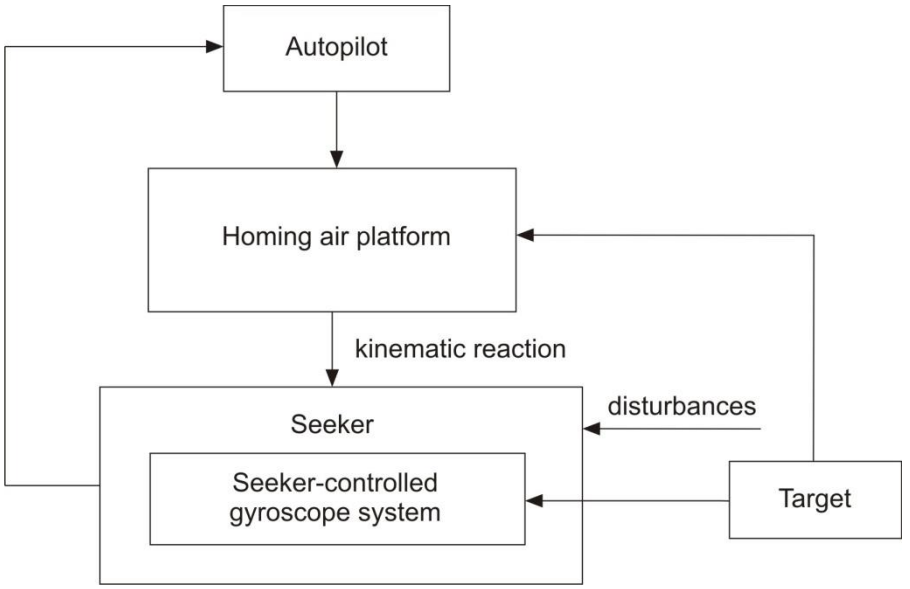

Fig. 1. Functional scheme of a gyroscope seeker system on a homing air platform

The seeker's axis is mounted on a ball joint and is capable of angular displacement (inclination). The purpose of the seeker is to (i) determine the angle between the seeker axis (SA) and the target line of sight (T-LOS) during the flight of the air platform (AP) and (ii) automatically equalize that angle (i.e. to automatically align the SA with the T-LOS), to allow the seeker to track the target.

The SA to T-LOS angle is a bias in the automatic target tracking process. When the SA tracks a target, i.e. the SA coincides with the T-LOS, then the SA to T-LOS angle is known. The SA to T-LOS angle is output to the AP autopilot, which in turn outputs appropriate commands to the AP controller system. The AP controller system actuates the control planes to achieve the required changes in the course of the AP [3].

Note that the design parameters of the gyroscope system alone cannot provide sufficient accuracy of the T-LOS position setting. In order to keep the T-LOS continuously aligned with the GS axis, optimum (given the adopted criterion of quality) parameters of the controller should be provided to minimize the dynamic effects applied to the system [4]. This work provides the results of tests that indicated that the best way to achieve this objective would be to implement a sliding mode controller in the gyroscope system.

2. EQUATIONS OF THE DYNAMICS OF THE MOBILE PLATFORM GYROSCOPE SYSTEM

Figure 2 presents an overview of the gyroscope system (GS) with the applied forces and force moments.

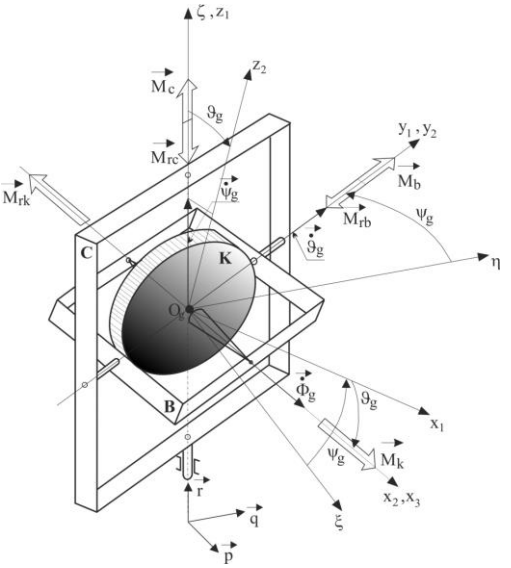

Fig. 2. Overview of the gyroscope system

The following coordinate systems were applied:

$O_o\xi\eta\varsigma$ – movable coordinate system with the origin on the mobile platform (the board of the air platform);

$O_g x_1 y_1 z_1$ – movable coordinate system with the origin on outer frame C;

$O_g x_2 y_2 z_2$ – movable coordinate system with the origin on inner frame B;

$O_g x_3 y_3 z_3$ – movable coordinate system with the origin on rotor K.

The other values in Fig. 2 are as follows: p,q,r – components of the mobile platform angular velocity vector; $\Phi_g, \vartheta_g, \psi_g$ – angles of own rotation, inner frame rotation and outer frame rotation, respectively; M_k, M_b, M_c – force moments applied to the rotor, the inner frame and the outer frame, respectively; M_{rk}, M_{rb}, M_{rc} – moments of friction forces within the mounting bearings and from the drag.

Lagrange second kind equations were used to derive the most generic equations of dynamics of the gyroscope system on the mobile platform:

$$\begin{aligned}
&\left(J_{y_2}+J_{y_3}\right)\frac{d}{dt}\omega_{gy_2}+\left(J_{x_2}-J_{z_2}-J_{z_3}\right)\omega_{gx_2}\omega_{gz_2}+J_{x_3}\omega_{gx_3}\omega_{gz_2}+\\
&-m_g l_g\frac{d}{dt}V_{gz_2}-m_g l_g\left[V_{gy_2}\omega_{gx_2}-V_{gx_2}\omega_{gy2}\right]=M_b-M_{rb}
\end{aligned} \tag{1}$$

$$\begin{aligned}
&J_{z_1}\frac{d}{dt}\omega_{gz_1}+\left(J_{y_1}-J_{x_1}\right)\omega_{gy_1}\omega_{gx_1}-J_{x_2}\frac{d}{dt}\left(\omega_{gx_2}\sin\vartheta_g\right)+\\
&+\left(J_{z_2}+J_{z_3}\right)\frac{d}{dt}\left(\omega_{gz_2}\cos\vartheta_g\right)-J_{x_2}\omega_{gx_2}\omega_{gy_1}\cos\vartheta_g+\\
&+\left(J_{y_2}+J_{y_3}\right)\omega_{gy_2}\omega_{gx_1}-\left(J_{z_2}+J_{z_3}\right)\omega_{gz_2}\omega_{gy_1}\sin\vartheta_g+\\
&-J_{x_3}\frac{d}{dt}\left(\omega_{gx_3}\sin\vartheta_g\right)-J_{x_3}\omega_{gx_3}\omega_{gy_1}\cos\vartheta_g+m_g l_g\frac{d}{dt}\left[V_{gy_2}\left(1+\cos\vartheta_g\right)\right]+\\
&+m_g l_g\left[V_{gx_2}\omega_{gx_1}\sin\vartheta_g-V_{gy_2}\omega_{gy_1}\sin\vartheta_g-V_{gz_2}\omega_{gx_1}\left(1+\cos\vartheta_g\right)\right]+\\
&+m_g l_g\left[V_{gx_1}\left(\omega_{gz_1}+\omega_{gz_2}\right)+V_{gy_1}\omega_{gy_2}\sin\vartheta_g\right]=M_c-M_{rc}
\end{aligned} \tag{2}$$

with:

$J_{x_1}, J_{y_1}, J_{z_1}$ – moments of inertia of the outer frame; $J_{x_2}, J_{y_2}, J_{z_2}$ – moments of inertia of the inner frame; $J_{x_3}, J_{y_3}, J_{z_3}$ – moments of inertia of the rotor; m_g – mass of the inner frame and rotor; l_g – distance from the GS mass centre to the GS centre of rotation; V_o – linear velocity of the mobile platform,

and:

$$\omega_{gx_1} = p\cos\psi_g + q\sin\psi_g;$$
$$\omega_{gy_1} = -p\sin\psi_g + q\cos\psi_g;$$
$$\omega_{gz_1} = \dot{\psi}_g + r;$$
$$\omega_{gx_2} = \omega_{gx_1}\cos\vartheta_g - \omega_{gz_1}\sin\vartheta_g;$$
$$\omega_{gy_2} = \omega_{gy_1} + \dot{\vartheta}_g;$$
$$\omega_{gz_2} = \omega_{gx_1}\sin\vartheta_g + \omega_{gz_1}\cos\vartheta_g;$$
$$\omega_{gx_3} = \omega_{gx_2} + \dot{\Phi}_g;$$
$$V_{gx_1} = V_o\cos\psi_g;$$
$$V_{gy_1} = -V_o\sin\psi_g;$$
$$V_{gx_2} = V_{gx1}\cos\vartheta_g + l_g\omega_{gy_1}\sin\vartheta_g;$$
$$V_{gy_2} = V_{gy1} + l_g\left(\omega_{gz_1} + \omega_{gz_2}\right);$$
$$V_{gz_2} = V_{gx1}\sin\vartheta_g - l_g\left(\omega_{gy_1}\cos\vartheta_g + \omega_{gy_2}\right).$$

It was assumed that the gyroscope system was astatic: $l_g = 0$, the moments of inertia of the frames could be ignored: $J_{x_1} = J_{y_1} = J_{z_1} = 0$; $J_{x_2} = J_{y_2} = J_{z_2} = 0$, the angles ϑ_g, ψ_g and the angular velocities $\dot{\vartheta}_g, \dot{\psi}_g$ of the GS axis were negligible; hence, the equations of motion (1) to (2) became:

$$J_{gk}\left(\ddot{\vartheta}_g + \dot{q}\right) + J_{go}n_g\left(r + \dot{\psi}_g\right) = M_b - M_{rb} \tag{3}$$
$$J_{gk}\left(\ddot{\psi}_g + \dot{r}\right) - J_{go}n_g\left(\dot{\vartheta}_g + q\right) = M_c - M_{rc} \tag{4}$$

with:

$J_{gk} = J_{y_3} = J_{z_3}$, $J_{go} = J_{x_3}$;

$M_{rb} = \eta_b\dot{\vartheta}_g$, $M_{rc} = \eta_c\dot{\psi}_g$;

$n_g = \dot{\Phi}_g = const$ – angular velocity of the rotor;

η_b, η_c – friction coefficients in the mounting bearings.

3. GYROSCOPE SYSTEM CONTROL

The control of the gyroscope system was defined by equations (1) to (4) and installed on the mobile platform and designed to be based on two controllers:

1. A proportional-derivative controller (PDC);
2. A sliding mode controller (SMC).

Figure 3 shows the functional control diagram of the gyroscope system installed on the mobile platform.

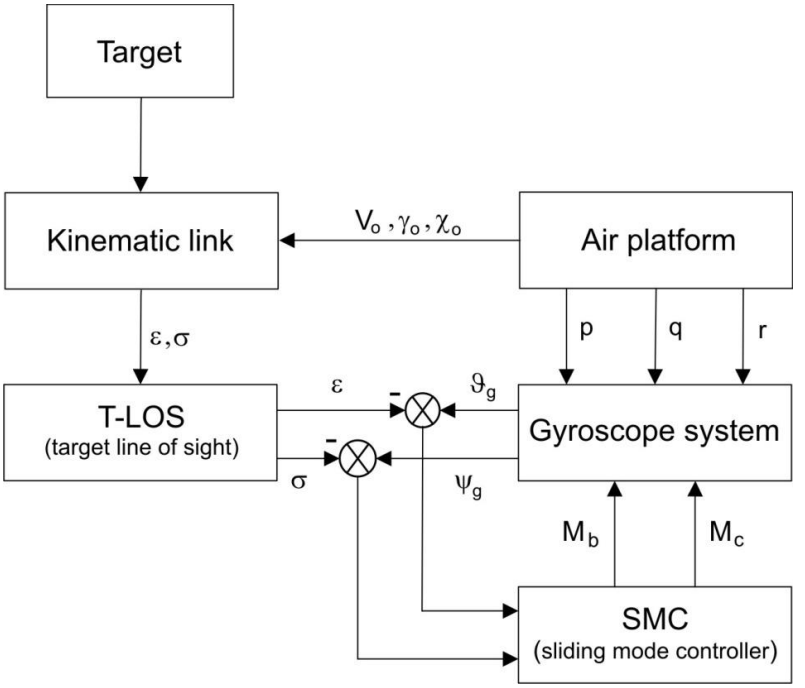

Fig. 3. Functional diagram of the gyroscope system control

PDC

The control law for the gyroscope system was developed in [1] and expressed as follows:

$$M_b = -k_b e_\vartheta + k_c e_\psi - h_g \dot{e}_\vartheta \tag{5}$$

$$M_c = -k_c e_\vartheta - k_b e_\psi - h_g \dot{e}_\psi \tag{6}$$

with:

ε, σ – spatial orientation angle of T-LOS;

$e_\vartheta = \vartheta_g - \varepsilon$; $\dot{e}_\vartheta = \dot{\vartheta}_g - \dot{\varepsilon}$; $e_\psi = \psi_g - \sigma$; $\dot{e}_\psi = \dot{\psi}_g - \dot{\sigma}$.

The PDC factors k_b, k_c, h_g were optimized due to the minimum bias between the set and actual trajectories.

The angles ε, σ of T-LOS position are the angle settings input to the control system during tracking of the detected target and derived with the following system of equations used to describe the relative positions of the air platform and the target:

$$\frac{d\xi}{dt} = V_c[\cos\chi_c \cos\sigma \cos(\varepsilon - \gamma_c) + \sin\chi_c \sin\sigma] + \\ - V_o[\cos\chi_o \cos\sigma \cos(\varepsilon - \gamma_o) + \sin\chi_o \sin\sigma] \tag{7}$$

$$\frac{d\varepsilon}{dt} = \frac{1}{\xi \cos\sigma}\{-V_c \cos\chi_c \sin(\varepsilon - \gamma_c) + V_o \cos\chi_o \sin(\varepsilon - \gamma)\} \tag{8}$$

$$\frac{d\sigma}{dt} = -\frac{1}{\xi}\{ V_c[\cos\chi_c \sin\sigma \cos(\varepsilon - \gamma_c) - \sin\chi_c \cos\sigma] + \\ - V_o[\cos\chi \sin\sigma \cos(\varepsilon - \gamma_o) - \sin\chi_o \cos\sigma] \} \tag{9}$$

with:

ξ – air platform distance to the target;

V_o, V_c – velocities of the air platform and the target;

χ_c, γ_c – yaw and pitch angles of the target velocity vector;

χ_o, γ_o – yaw and pitch angles of the air platform velocity vector.

As the air platform approaches the target, the pitch and yaw angles γ_o, χ_o change as defined by the following relations (i.e. the proportional navigation algorithm):

$$\dot{\gamma}_o = a_1 \dot{\vartheta}_g \tag{10a}$$

$$\dot{\chi}_o = a_2 \dot{\psi}_g \tag{10b}$$

with:

a_1, a_2 – proportional navigation constants.

Sliding mode controller (SMC)

Sliding mode control is a type of robust control. The main advantage of sliding mode control is its insensitivity to external and internal interference [5, 6]. Moreover, a sliding mode controller (SMC) has a simple design and can be applied with highly non-linear systems, such as the gyroscope system investigated here [7]. Two sliding surfaces were defined:

$$s_{g1} = \dot{e}_\theta + \lambda_1 e_\theta \tag{11a}$$

$$s_{g2} = \dot{e}_\psi + \lambda_2 e_\psi \tag{11b}$$

where: λ_1, λ_2 – positive constants.

The slide mode control was determined with the following formulas:

$$M_b = -K_1 \operatorname{sgn}(s_{g1}) + M_{beq} \tag{12}$$

$$M_c = -K_2 \operatorname{sgn}(s_{g2}) + M_{ceq} \tag{13}$$

where:

M_{beq}, M_{ceq} – equivalent controls;

K_1, K_2 – sliding gain.

The equivalent controls were determined by equating the control surface differential coefficient to zero, i.e. $\dot{s}_{g1} = 0$ and $\dot{s}_{g2} = 0$.

To reduce chatter, the signum function was replaced with a saturation function [8, 9].

$$M_b = -K_1 \text{sat}(s_{g1}/\phi) + M_{beq} \tag{14}$$

$$M_c = -K_2 \text{sat}(s_{g2}/\phi) + M_{ceq} \tag{15}$$

where:

ϕ – thickness of the boundary layer.

4. TEST RESULTS

The simulation testing of the controlled gyroscope system dynamics included the following input parameters:

- velocity and initial position of the air platform
$$V_o = 500\,\text{m/s},\ X_o = 0\,\text{m},\ Y_o = 0\,\text{m},\ Z_o = 0\,\text{m}$$
- velocity and initial position of the target
$$V_c = 250\,\text{m/s},\ X_c = 1000\,\text{m},\ Y_c = 2000\,\text{m},\ Z_c = 500\,\text{m}$$
- angular velocity of the target velocity vector $\Omega_c = 0.1\,\text{rad/s}$
- proportional navigation constants $a_1 = a_2 = 3.5$
- parameters of the gyroscope system
$$J_{x_1} = 2.5 \cdot 10^{-5}\,\text{kgm}^2,\ J_{y_1} = J_{x_1},\ J_{z_1} = J_{x_1}$$
$$J_{x_2} = 5 \cdot 10^{-5}\ \text{kgm}^2,\ J_{y_2} = J_{x_2},\ J_{z_2} = J_{x_2}$$
$$J_{x_3} = 5 \cdot 10^{-4}\ \text{kgm}^2,\ J_{y_3} = 2.5 \cdot 10^{-4}\ \text{kgm}^2,\ J_{z_3} = J_{y_3}$$
$$m_g = 0.24\,\text{kg},\ n_g = 600\ \text{rad/s},\ \eta_b = \eta_c = 0.01\ \text{Nm/s}$$
- gain factors of the PDC
$$k_b = 31.48,\ k_c = -2.986,\ h_g = 31.525$$
- gain factors of the SMC
$$\lambda_1 = 75,\ K_1 = 15,\ \lambda_2 = 150,\ K_2 = 15,\ \phi = 1$$

The kinematic input functions of the air platform (a rocket missile) affecting the gyroscope system were adopted in a harmonic form:

$$p = p_o \sin(\nu t),\ q = q_o \cos(\nu t),\ r = r_o \sin(\nu t)$$

with: $p_o = 5\,\text{rad/s}$, $q_o = 5\,\text{rad/s}$, $r_o = 5\,\text{rad/s}$, $\nu = 15\,\text{rad/s}$.

The tests were carried out in Matlab/Simulink with an integration step dt = 0.00001 [10].

Figures 4 to 7 show the simulation test results for the PDC (see left) and the SMC (see right) applied to control a non-linear gyroscope system defined with the equations (1-2) at $l_g = 0.001$ m.

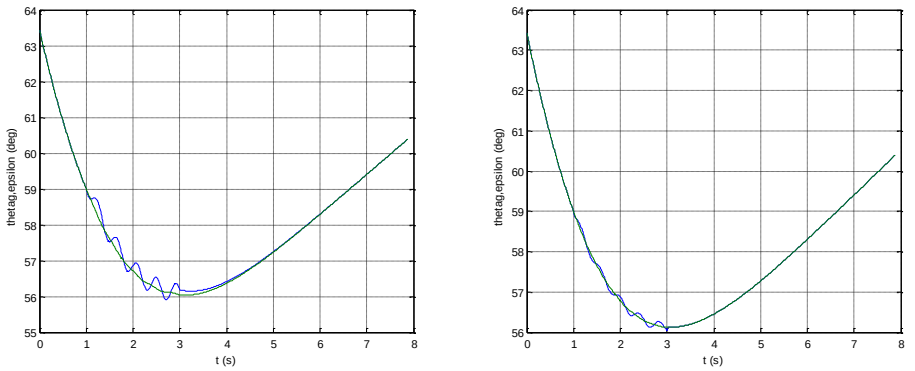

Fig. 4. Variations in time of the pitch angles ϑ_g and ε

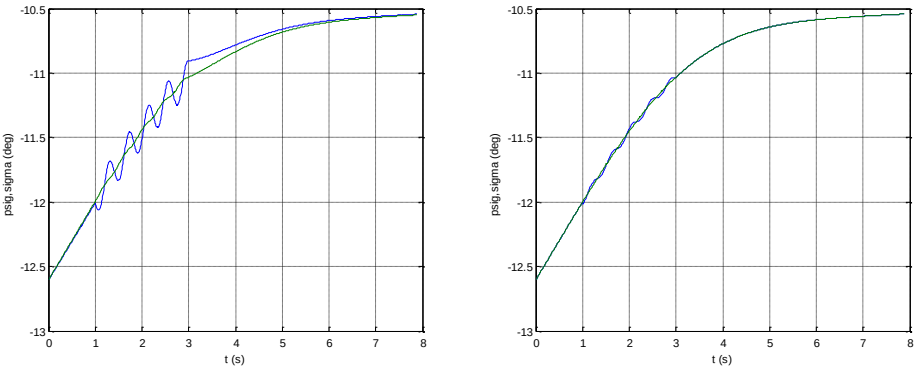

Fig. 5. Variations in time of the yaw angles ψ_g and σ

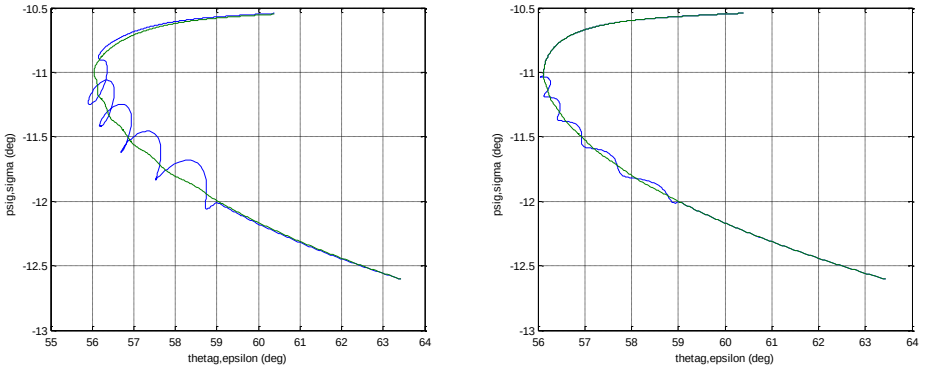

Fig. 6. Trajectories of the T-LOS and GS axis

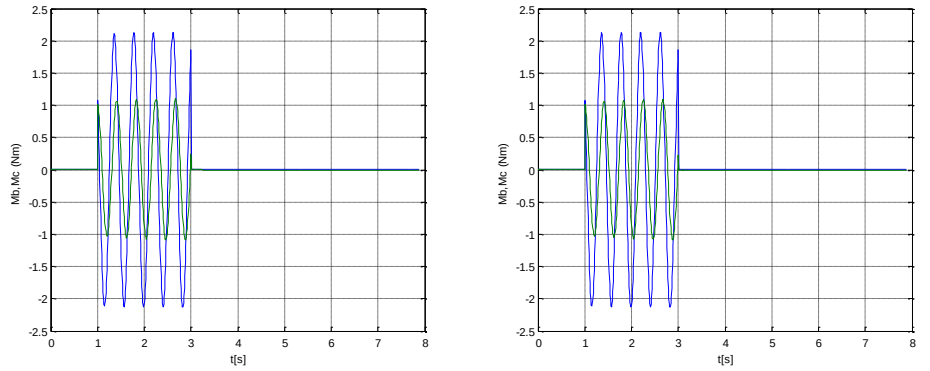

Fig. 7. Control moments

Figures 8 to 11 show the simulation test results for the PDC (see left) and the SMC (see right) applied to control a non-linear gyroscope system defined with the equations (1-2) at $l_g = 0.005$ m.

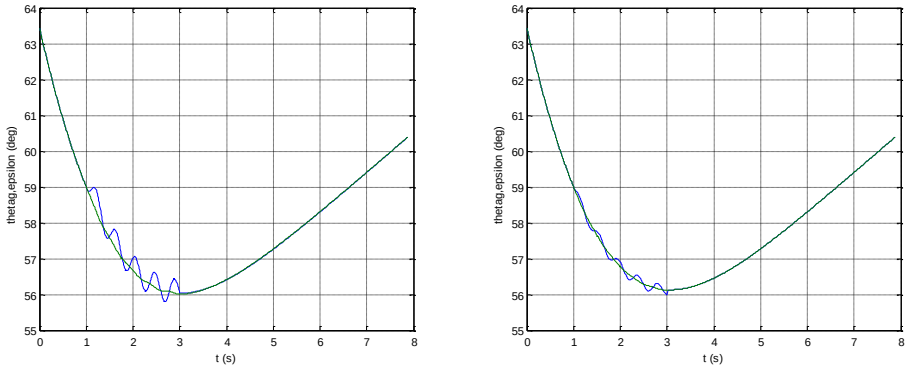

Fig. 8. Variations in time of the pitch angles ϑ_g and ε

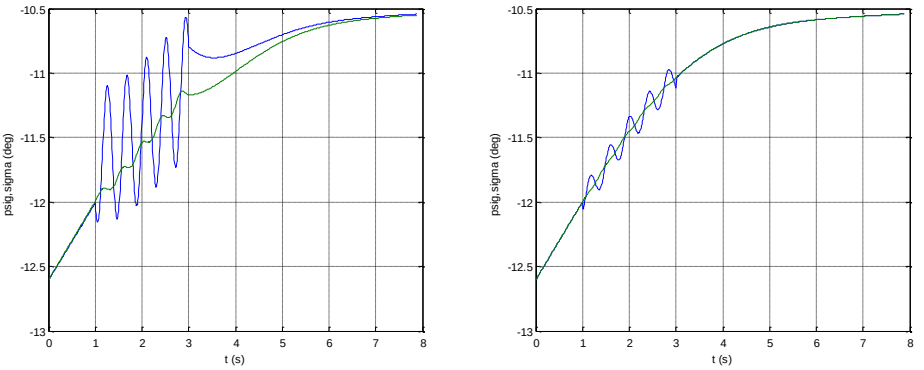

Fig. 9. Variations in time of the yaw angles ψ_g and σ

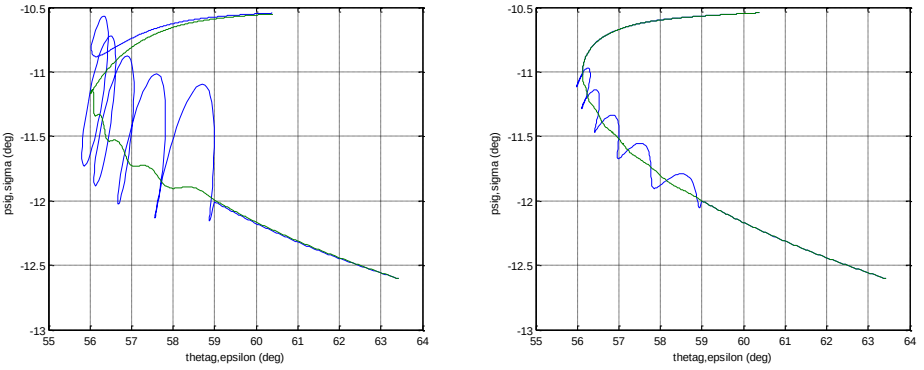

Fig. 10. Trajectories of the T-LOS and GS axis

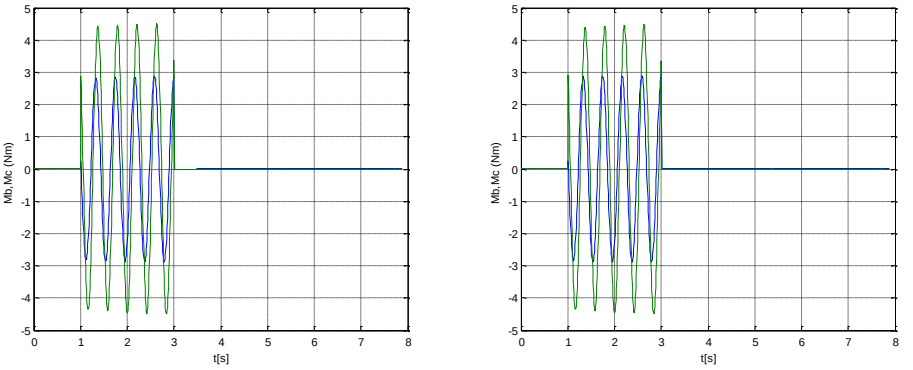

Fig. 11. Control moments

5. CONCLUSION

The numerical simulation test results demonstrated the high effectiveness of the sliding mode control applied to the gyroscope system of the seeker for the hypothetical air platform. This is evident in the right-hand columns of the charts in Figs. 4 to 6 and 8 to 10. The quantitative tests used a mean-square error of bias criterion from the settings. The performance of the SMC was approximately 10% better than in the PDC. This is critical for the precise determination of the location of a target identified by an unmanned air platform and intended to be destroyed by a specific type of precision strike weapon. The case for controlling the gyroscope system of a target seeker in a homing missile was similar: the sliding mode controller provided the most stable tracking of a manoeuvring air target, even with transient disturbances occurring within the homing missile.

The further research work requires experimental tests, initially in a laboratory setting followed by test range experiments, to confirm the simulation test results provided by the work presented here.

REFERENCES

[1] Awrejcewicz Jan, Zbigniew Koruba. 2012. *Classical Mechanics: Applied Mechanics and Mechatronics*. New York: Springer.

[2] Krzysztofik Izabela, Zbigniew Koruba. 2014. "Mathematical Model of Movement of the Observation and Tracking Head of an Unmanned Aerial Vehicle Performing Ground Target Search and Tracking". *Journal of Applied Mathematics* 11 pages, Article ID 934250.

[3] Gapiński Daniel, Izabela Krzysztofik, Zbigniew Koruba. 2014. "Analysis of the dynamics and control of the modified optical target seeker used in anti-aircraft rocket missiles". *Journal of Theoretical and Applied Mechanics* 52 (3): 629-639.

[4] Wang Cheng-Chi, Her-Terng Yau. 2011. "Nonlinear dynamic analysis and sliding mode control for a gyroscope system". *Nonlinear Dynamics* 66 : 53-65.

[5] Utkin Vadim. 2008. Sliding Mode Control: Mathematical Tools, Design and Applications. In *Nonlinear and Optimal Control Theory*, 289-347, Springer.

[6] Tomera Mirosław. 2009. "Projekt regulatora nieliniowego dla autopilota statku". *Zeszyty Naukowe Akademii Morskiej w Gdyni* 62 : 223-233.

[7] Bachman Paweł. 2004. Zastosowanie algorytmu SMC do sterowania serwomechanizmów elektrohydraulicznych. *X Jubileuszowe Seminarium „Napędy i sterowanie 2004"*, 388-391. Gdynia: Wydawnictwo Akademii Morskiej.

[8] Szymak Piotr. 2010. "Selection of Methods for Underwater Robot Control". *Solid State Phenomena* 164 : 149-154.

[9] Utkin Vadim, Jürgen Guldner, Jingxin Shi. 2009. *Sliding Mode Control in Electro-Mechanical Systems*. Boca Raton: CRC Press.

[10] Baranowski Leszek. 2013. "Effect of the mathematical model and integration step on the accuracy of the results of computation of artillery projectile flight parameters". *Bulletin of the Polish Academy of Sciences: Technical Sciences* 61 (2) : 475-484.

Sterowanie ślizgowe układem giroskopowym

Izabela KRZYSZTOFIK, Zbigniew KORUBA

Politechnika Świętokrzyska,
Aleja Tysiąclecia Państwa Polskiego 7, 25-314 Kielce

Streszczenie. W pracy przedstawiono model matematyczny układu giroskopowego wraz z regulatorem ślizgowym. Analiza porównawcza różnych algorytmów sterowania zastosowanych w sterowanym układzie giroskopowym umieszczonym na ruchomej podstawie (np. na pokładzie bezzałogowego aparatu latającego lub samonaprowadzającego pocisku rakietowego) wykazała, że najbardziej efektywne jest sterowanie ślizgowe, zwłaszcza w warunkach występowania zakłóceń zewnętrznych i kinematycznego oddziaływania podłoża. Tego rodzaju układ może znaleźć zastosowanie w optycznych koordynatorach celu broni precyzyjnego rażenia. Wyniki badań symulacyjnych przedstawione zostały w graficznej postaci.
Słowa kluczowe: mechanika, giroskop sterowany, regulator ślizgowy, dynamika, sterowanie